

Poststack migration of P-SV data

Mark P. Harrison

ABSTRACT

This paper deals with the application of poststack migration to P-SV data. It is shown that P-SV diffractions in a vertically-inhomogeneous medium are hyperbolic to first order, and an expression for their migration velocity can be obtained. The resulting velocities are 6-11% less than the P-SV RMS velocities. In synthetic P-SV data it is found that asymmetric dispersal creates a strong splitting of diffraction tails at shallow depths. This splitting is removed by application of depth-variant P-SV DMO. Migration of the DMO-corrected synthetic P-SV stack data using a conventional phase-shift algorithm and the migration velocity function adequately collapses diffractions, whereas migration using the RMS velocity function gives significant overcorrection.

INTRODUCTION

The use of appropriate normal moveout (NMO) corrections, coupled with P-SV dip moveout (DMO) allow the construction of stack sections that are zero-offset in the kinematic sense. An obvious extension to converted-wave processing is to apply some sort of post-stack migration to these sections, in order to properly position dipping reflectors and collapse diffractions. Various authors (e.g., Garotta, 1986) have shown migrated P-SV stack sections, but the question of the applicability of P-SV post-stack migration has not yet been addressed, except for the constant-velocity case (Eaton and Stewart, 1989; Eaton et. al., 1991). The purpose of this paper is to establish the shape of P-SV diffractions from point scattering in a multi-layered medium, and derive a velocity function which will properly migrate them. As the migration process can be thought of as a 2-D deconvolution process in which the point-response function is removed (Brouwer et. al., 1985), adequately migrating a diffraction curve is equivalent to removing the point-response function, and ensures correct migration of all other data.

To test the accuracy of the migration velocity equation presented here, poststack migration is applied to synthetic data sets containing reflections from a number of point diffractors. These data were stacked using both the depth-variant binning method (Eaton et. al., 1990) and P-SV DMO (Harrison, 1990). The resulting sections are migrated using the migration velocity equation developed here as well as the RMS stacking velocities (Tessmer and Behle, 1988). For the remainder of this paper the depth-variant binning method will be abbreviated as DVBM.

THEORY

Consider conversion from the point diffractor shown in Figure 1. The point is at distance x away from the surface CCP position, where both the source and receiver are located. Energy travels from the source to the point along the path segments a_i with

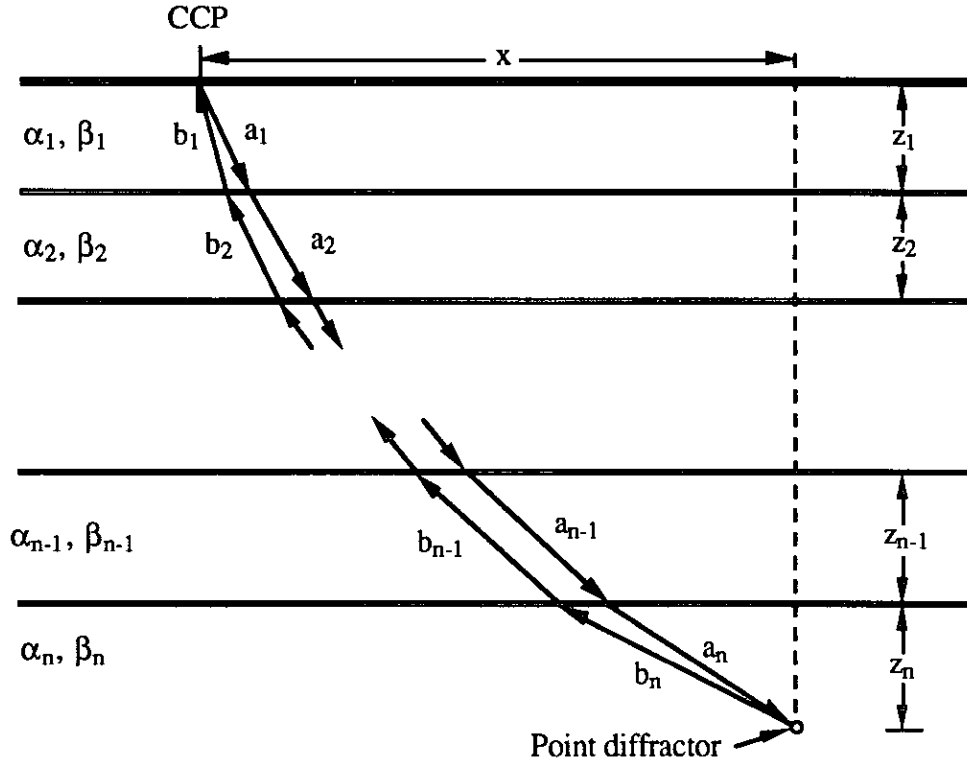


FIG. 1. Zero-offset raypaths traveled through a layered Earth from a point diffractor.

velocity α_i , and back from the point along the path segments b_i with velocity β_i . The total traveltime t is

$$t = \sum_{i=1}^n \frac{a_i}{\alpha_i} + \sum_{i=1}^n \frac{b_i}{\beta_i}. \quad (1)$$

For the downward path, the ray parameter p_1 is constant, and for the upward path the second ray parameter p_2 is constant. The total horizontal distance traveled along both up-going and down-going paths is equal to the offset x ;

$$x = p_1 \sum_{i=1}^n \frac{\alpha_i z_i}{\sqrt{1-p_1^2 \alpha_i^2}} = p_2 \sum_{i=1}^n \frac{\beta_i z_i}{\sqrt{1-p_2^2 \beta_i^2}}. \quad (2)$$

Because the ray parameters are seen to satisfy different equations, they must, in general, be different. This means that the upward and downward raypaths are also different, and the exploding reflector model (Loewenthal et al., 1976) does not strictly hold for P-SV data. In terms of the two ray parameters, equation 1 can be rewritten as

$$t = \sum_{i=1}^n \frac{z_i}{\alpha_i \sqrt{1-p_1^2 \alpha_i^2}} + \sum_{i=1}^n \frac{z_i}{\beta_i \sqrt{1-p_2^2 \beta_i^2}}. \quad (3)$$

To obtain an approximate solution for t , a Taylor's series expansion can be performed about $x = 0$ (the small diffractor offset case);

$$t \cong t_0 + x \left(\frac{dt}{dx} \right)_{x=0} + \frac{x^2}{2} \left(\frac{d^2t}{dx^2} \right)_{x=0} + \frac{x^3}{6} \left(\frac{d^3t}{dx^3} \right)_{x=0} + O(x^4), \quad (4)$$

where $O(x^4)$ represents terms of order x^4 and higher, and t_0 is again the two-way vertical traveltine given by

$$\begin{aligned} t_0 &= \sum_{i=1}^n \left(\frac{\alpha_i + \beta_i}{\alpha_i \beta_i} \right) z_i \\ &= \sum_{i=1}^n \tau_i. \end{aligned} \quad (5)$$

τ_i is the two-way vertical traveltine through the i 'th layer. The total derivative of t w.r.t. x is

$$\frac{dt}{dx} = \frac{\partial t}{\partial p_1} \frac{dp_1}{dx} + \frac{\partial t}{\partial p_2} \frac{dp_2}{dx}. \quad (6)$$

Differentiating equation 2 w.r.t. p_1 and p_2 gives

$$\frac{dx}{dp_1} = \sum_{i=1}^n \frac{\alpha_i z_i}{(1-p_1^2 \alpha_i^2)^{3/2}} \quad (7)$$

and

$$\frac{dx}{dp_2} = \sum_{i=1}^n \frac{\beta_i z_i}{(1-p_2^2 \beta_i^2)^{3/2}}. \quad (8)$$

Differentiating equation 3 w.r.t. p_1 gives

$$\frac{\partial t}{\partial p_1} = p_1 \sum_{i=1}^n \frac{\alpha_i z_i}{(1-p_1^2 \alpha_i^2)^{3/2}} = p_1 \frac{dx}{dp_1}, \quad (9)$$

where equation 7 has been used. This gives

$$\frac{\partial t}{\partial p_1} \frac{dp_1}{dx} = p_1 . \quad (10)$$

Similarly

$$\frac{\partial t}{\partial p_2} \frac{dp_2}{dx} = p_2 , \quad (11)$$

and equation 6 becomes

$$\frac{dt}{dx} = p_1 + p_2 . \quad (12)$$

Equation 12 restates the definition of the ray parameter as the horizontal component of the slowness vector (Slotnick, 1959). At $x = 0$, both ray parameters are also zero, i.e.,

$$\left(\frac{dt}{dx} \right)_{x=0} = 0. \quad (13)$$

Differentiating equation 12 w.r.t. x results in

$$\begin{aligned} \frac{d^2t}{dx^2} &= \frac{dp_1}{dx} + \frac{dp_2}{dx} \\ &= \left[\sum_{i=1}^n \frac{\alpha_i z_i}{(1-p_1^2 \alpha_i^2)^{3/2}} \right]^{-1} + \left[\sum_{i=1}^n \frac{\beta_i z_i}{(1-p_2^2 \beta_i^2)^{3/2}} \right]^{-1} \end{aligned} \quad (14)$$

where equations 7 and 8 have been used. At $x = 0$, equation 14 becomes

$$\begin{aligned} \left(\frac{d^2t}{dx^2} \right)_{x=0} &= \left(\sum_{i=1}^n \alpha_i z_i \right)^{-1} + \left(\sum_{i=1}^n \beta_i z_i \right)^{-1} \\ &= \frac{\sum_{i=1}^n \alpha_i \beta_i \tau_i}{\left(\sum_{i=1}^n \frac{\alpha_i^2 \beta_i}{\alpha_i + \beta_i} \tau_i \right) \left(\sum_{i=1}^n \frac{\alpha_i \beta_i^2}{\alpha_i + \beta_i} \tau_i \right)} . \end{aligned} \quad (15)$$

Differentiating equation 14 w.r.t. x gives

$$\frac{d^3t}{dx^3} = \frac{d^2p_1}{dx^2} + \frac{d^2p_2}{dx^2}$$

$$= -3p_1 \frac{\left[\sum_{i=1}^n \frac{\alpha_i^3 z_i}{(1-p_1^2 \alpha_i^2)^{5/2}} \right]}{\left[\sum_{i=1}^n \frac{\alpha_i z_i}{(1-p_1^2 \alpha_i^2)^{3/2}} \right]^3} - 3p_2 \frac{\left[\sum_{i=1}^n \frac{\beta_i^3 z_i}{(1-p_1^2 \beta_i^2)^{5/2}} \right]}{\left[\sum_{i=1}^n \frac{\beta_i z_i}{(1-p_1^2 \beta_i^2)^{3/2}} \right]^3}, \quad (16)$$

and

$$\left(\frac{d^3 t}{dx^3} \right)_{x=0} = 0. \quad (17)$$

Using equations 13, 15, and 17, equation 14 becomes

$$t = t_0 + \frac{x^2}{2} \left[\frac{\sum_{i=1}^n \alpha_i \beta_i \tau_i}{\left(\sum_{i=1}^n \frac{\alpha_i^2 \beta_i}{\alpha_i + \beta_i} \tau_i \right) \left(\sum_{i=1}^n \frac{\alpha_i \beta_i^2}{\alpha_i + \beta_i} \tau_i \right)} \right] + O(x^4). \quad (18)$$

Squaring both sides of equation 18 gives

$$t^2 = t_0^2 + x^2 \left[\frac{t_0 \sum_{i=1}^n \alpha_i \beta_i \tau_i}{\left(\sum_{i=1}^n \frac{\alpha_i^2 \beta_i}{\alpha_i + \beta_i} \tau_i \right) \left(\sum_{i=1}^n \frac{\alpha_i \beta_i^2}{\alpha_i + \beta_i} \tau_i \right)} \right] + O(x^4). \quad (19)$$

Comparing equation 19 to the standard equation for the diffraction hyperbola,

$$t^2 = t_0^2 + \frac{4x^2}{V^2}, \quad (20)$$

where V is the migration velocity, it is seen that for P-SV data

$$V = 2 \sqrt{\frac{\left(\sum_{i=1}^n \frac{\alpha_i^2 \beta_i}{\alpha_i + \beta_i} \tau_i \right) \left(\sum_{i=1}^n \frac{\alpha_i \beta_i^2}{\alpha_i + \beta_i} \tau_i \right)}{t_0 \sum_{i=1}^n \alpha_i \beta_i \tau_i}}. \quad (21)$$

For the single-layer case, where $n=1$, equation 21 reduces to

$$\frac{1}{V} = \frac{1}{2} \left(\frac{1}{\alpha} + \frac{1}{\beta} \right). \quad (22)$$

Equation 22 is the same result given by Eaton et al. (1991).

Equation 19 shows that, to first order, P-SV diffraction curves are also hyperbolic, and that a P-SV stack section can be migrated using the velocity function defined by equation 21. This argument is only correct in a ray-theoretical sense, but it does give justification to applying post-stack migration to P-SV data.

Equation 21 can be compared to the P-SV RMS velocity function given by Tessmer and Behle (1988);

$$V_{\text{RMS}} = \sqrt{\frac{\sum_{i=1}^n \alpha_i \beta_i \tau_i}{t_0}} \quad (23)$$

The form of the RMS and migration velocity equations is seen to be significantly different. For the case of constant V_p/V_s ratio, the ratio of RMS velocity to migration velocity reduces to

$$\begin{aligned} \frac{V_{\text{RMS}}}{V_{\text{MIG}}} &= \frac{\alpha + \beta}{2\sqrt{\alpha\beta}} \\ &= \frac{\gamma + 1}{2\sqrt{\gamma}}, \quad \gamma = \frac{\alpha}{\beta} \end{aligned} \quad (24)$$

The function defined by equation 24 is plotted in Figure 2 for a range of V_p/V_s ratios. It is seen that the migration velocity is always less than the RMS velocity for realistic values of γ .

METHOD

Two sets of synthetic data were made to evaluate the migration velocity equation. The geometry parameters used in generating synthetic shot records are summarized in Table 1. The total data volume in both cases consisted of 41 records of 121 traces each.

Each source record was constructed by performing 2-D ray-tracing through the medium to compute the response to a number of point diffractors located at various depths beneath SP 181. The first sourcepoint was located at SP 101, and the last at SP 261. Diffraction amplitudes were computed using the following equation derived by Knopoff (1959);

$$A(r) = \frac{\gamma^2 \sin \theta}{\alpha(1+2\gamma^2)} \frac{A_0}{r} \quad (25)$$

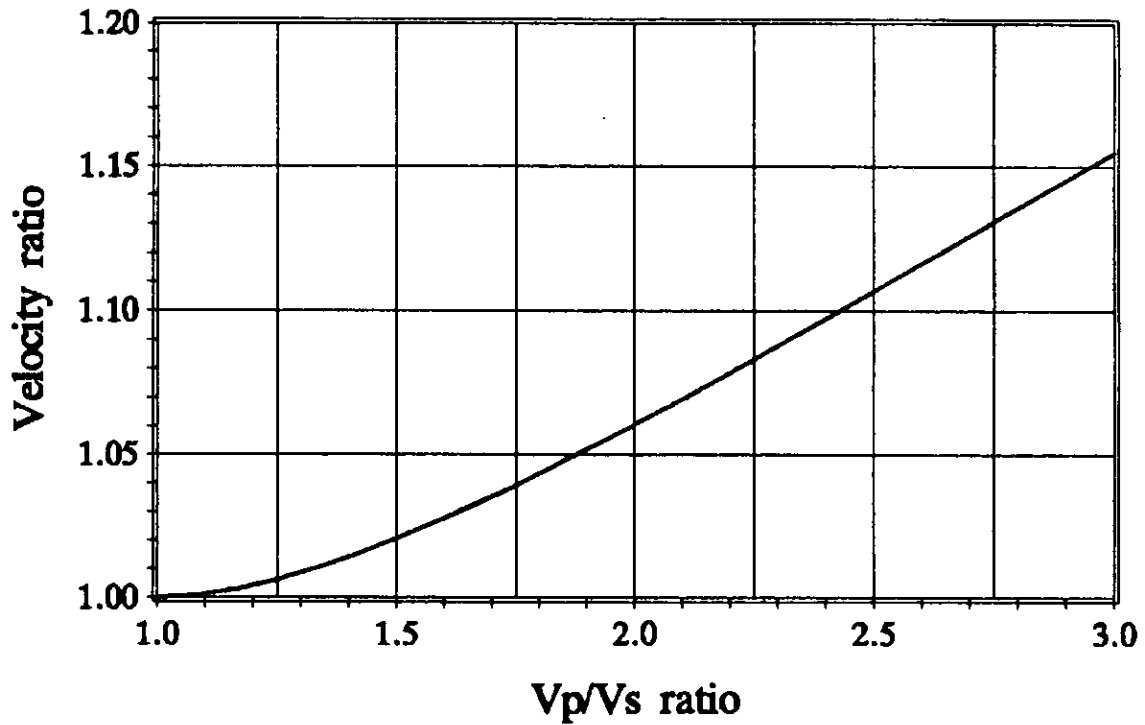


FIG. 2. Ratio of RMS velocity to migration velocity as a function of the V_p/V_s ratio for the constant-velocity case.

Table 1. Parameters used in generating the synthetic test data.

Group interval	25 meters
Source interval	100 meters
Traces per record	121
Trace offsets	0 to 1500 m, 25 m increment split-spread records
Nominal fold	15
Data bandwidth	8-35 Hz
Record length	3500 ms
Sample rate	2 ms

where

A_0 = initial wavelet amplitude,
 r = length of source-to-receiver travelpath, and
 θ = angle between the incident and reflected rays.

The first data set was created using eight point diffractors positioned at depths ranging from 250 m to 2.0 km, embedded in a medium with P-wave velocity 3000 m/s and

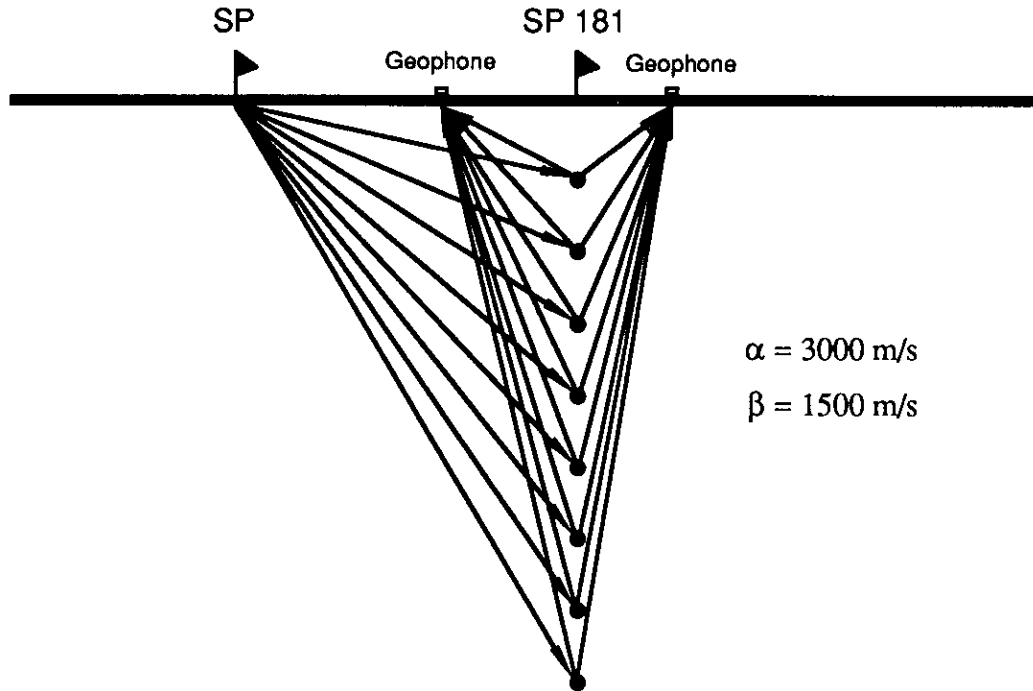


FIG. 3. Sample raypaths for diffracted energy received by two geophones. Diffractors are positioned at 250 m depth intervals, ranging from 250 m to 2000 m.

S-wave velocity 1500 m/s (Figure 3). The resulting traces were moveout corrected using ray-traced NMO and scaled to compensate for spherical divergence. Several of these records are displayed in Figure 4.

After NMO and gain, the data were stacked using DVBM and P-SV DMO, giving the results shown in Figures 5 and 6. The DMO section is seen to better preserve the diffraction tails, and was used as input to a phase-shift migration program (Gadzag, 1978) using both the RMS velocity function of equation 23 and the migration velocity function defined by equation 22. The diffractions are seen to be overmigrated using the RMS velocities (Figure 7), but successfully collapsed using the migration velocity (Figure 8). For this simple case equation 22 is exact, and the results shown in Figure 8 are the best that can be obtained for the geometry and wavelet bandwidth used.

As a more appropriate test of equation 21, a second set of synthetic records was created. The model for this case consists again of a number of point diffractors, but embedded in a layered media having thirty-two different velocity intervals. The layer thickness and velocity values are based on a blocked sonic log from the Carrot Creek field of Alberta (Nazar, 1990), and are plotted vs. two-way P-SV time in Figure 9. Also shown is the ratio of RMS and migration velocities, from which it is seen that the RMS velocities are about 6-11% greater than the migration velocities. Sample records are shown in Figure 10, again with ray-traced NMO and geometric spreading compensation applied.

The second data set was stacked using DVBM (Figure 11) and depth-variant P-SV DMO (Figure 12). The DVBM stack shows significant distortion and attenuation of the earlier diffractions. These early diffractions are also seen to split into two components. This splitting is due to the asymmetry of dispersal that occurs between data from

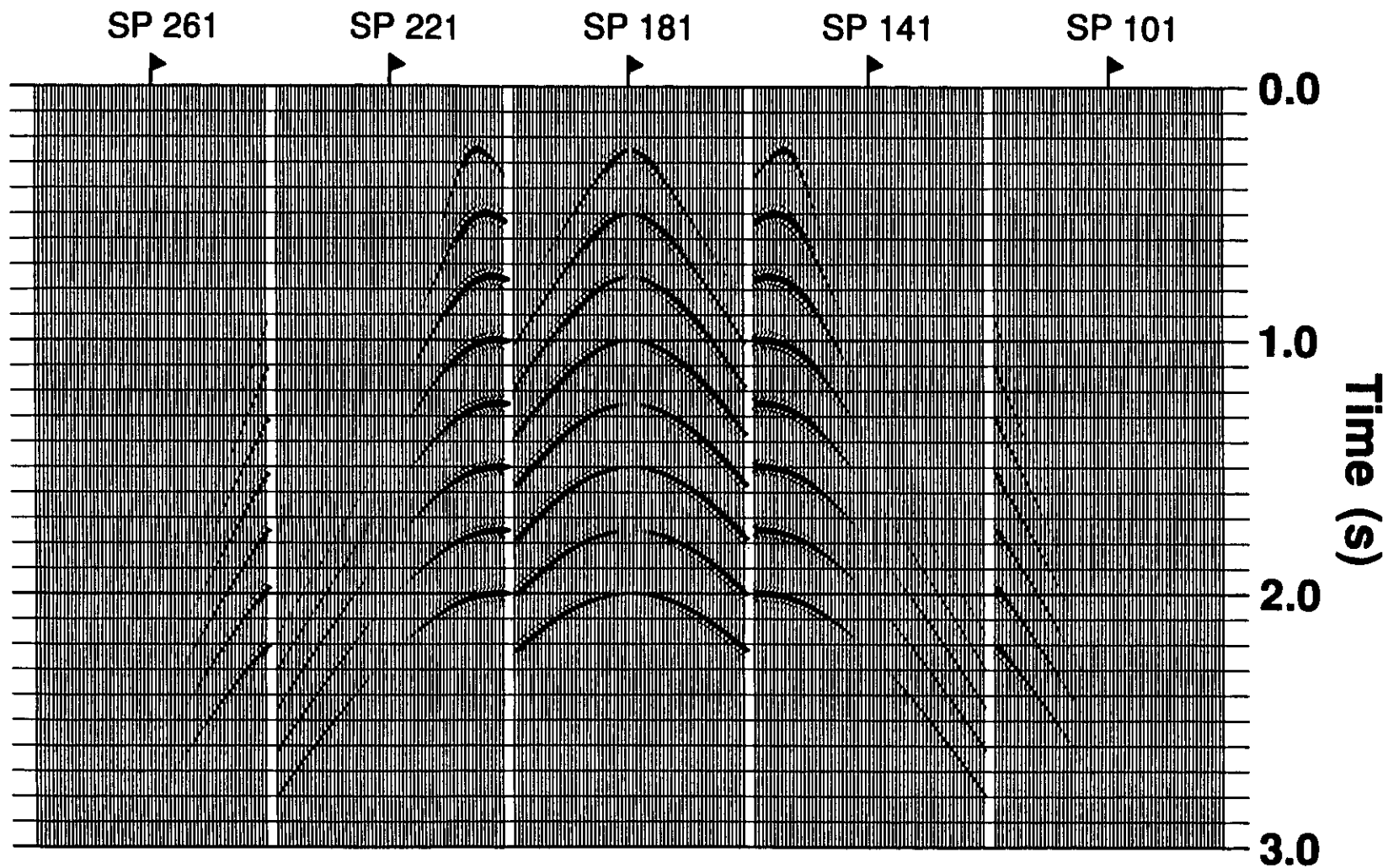


FIG. 4. Sample synthetic P-SV records for the constant-velocity case (every second trace). The data have been NMO corrected and scaled for spherical divergence.

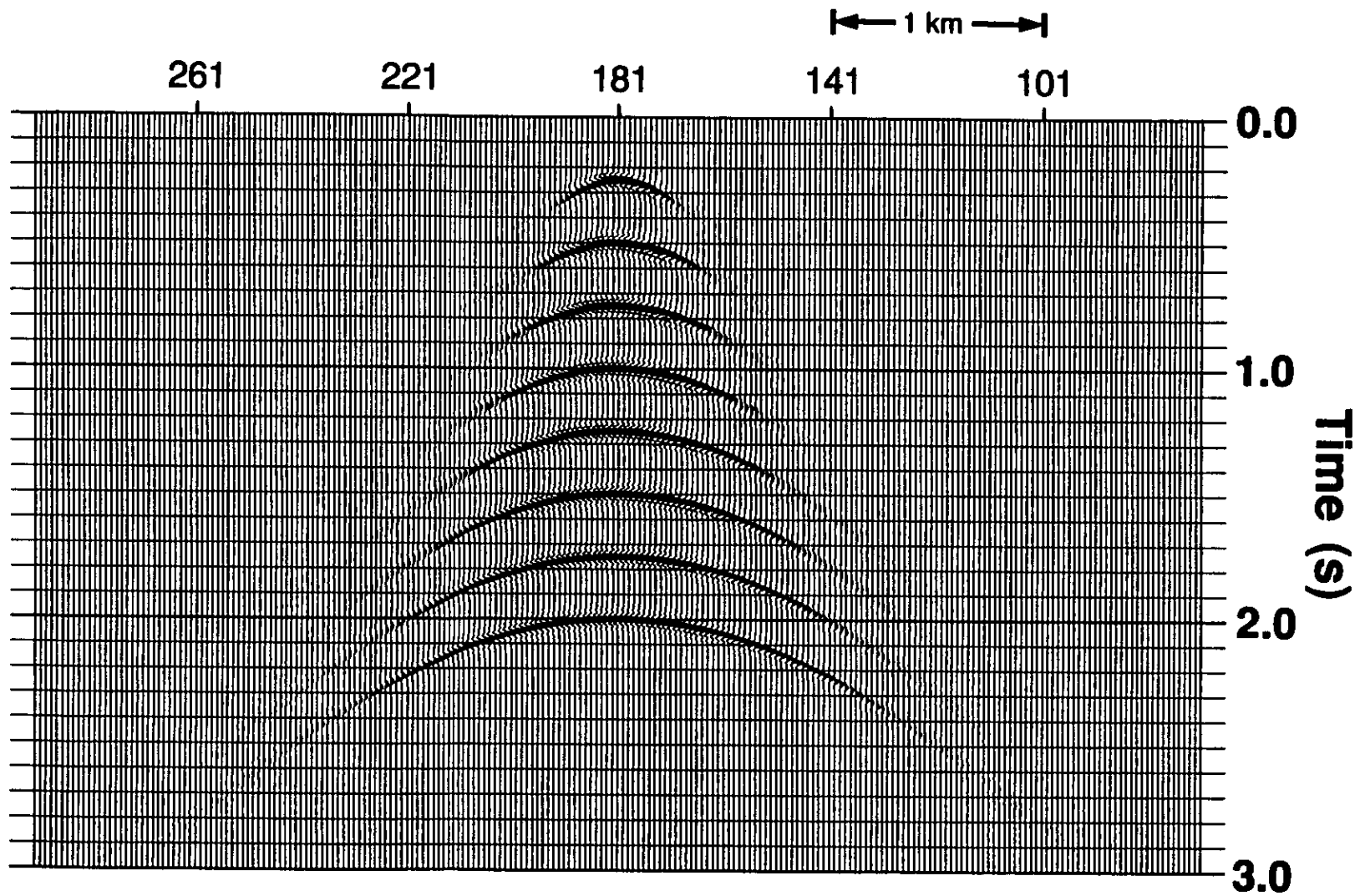


FIG. 5. Constant-velocity data stacked using DVBM (every second trace).

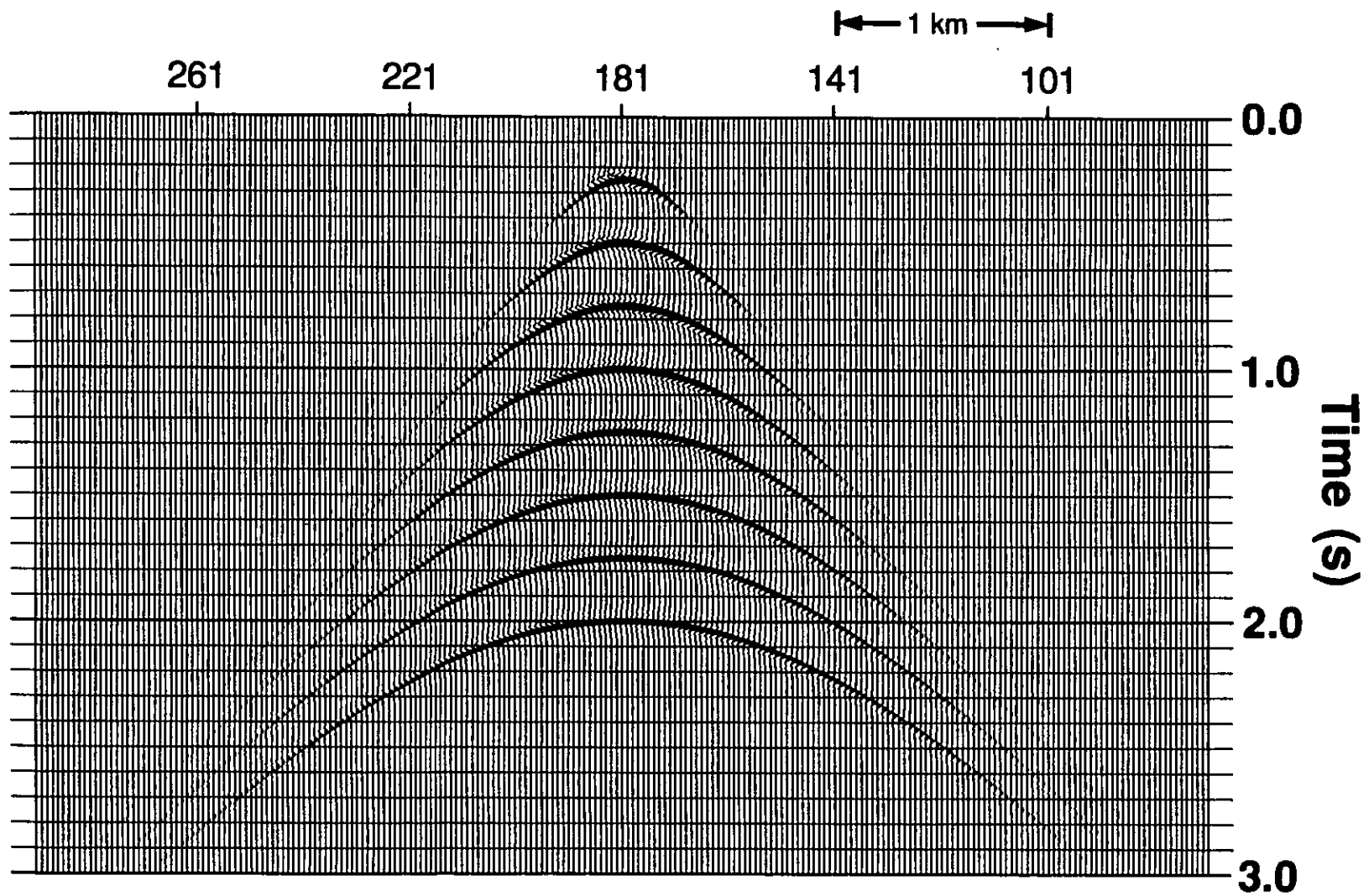


FIG. 6. Constant-velocity data stacked using P-SV DMO (every second trace).

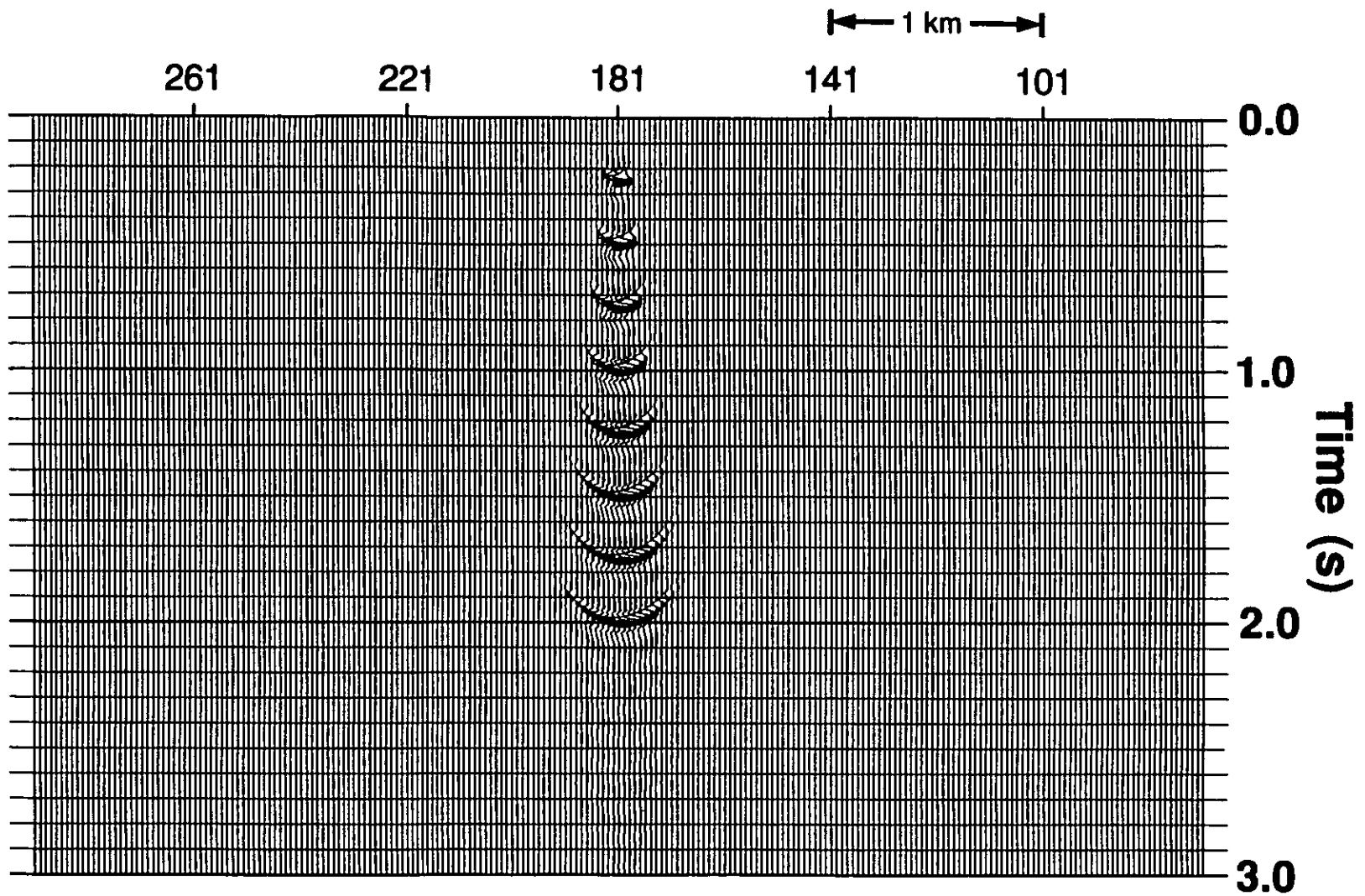


FIG. 7. DMO-stacked constant-velocity data migrated using the RMS velocity function (every second trace).

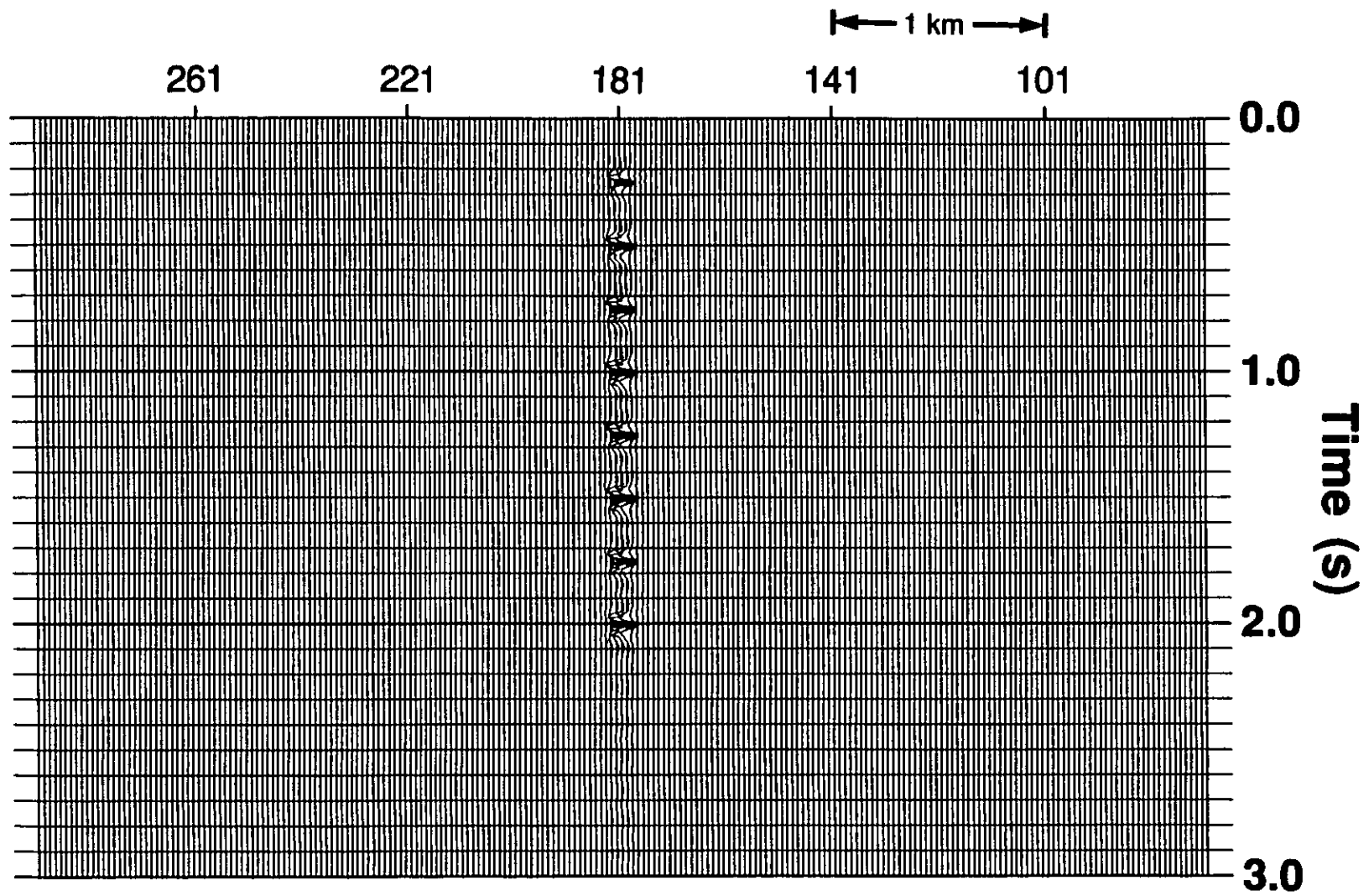


FIG. 8. DMO-stacked constant-velocity data migrated using the migration velocity function (every second trace).

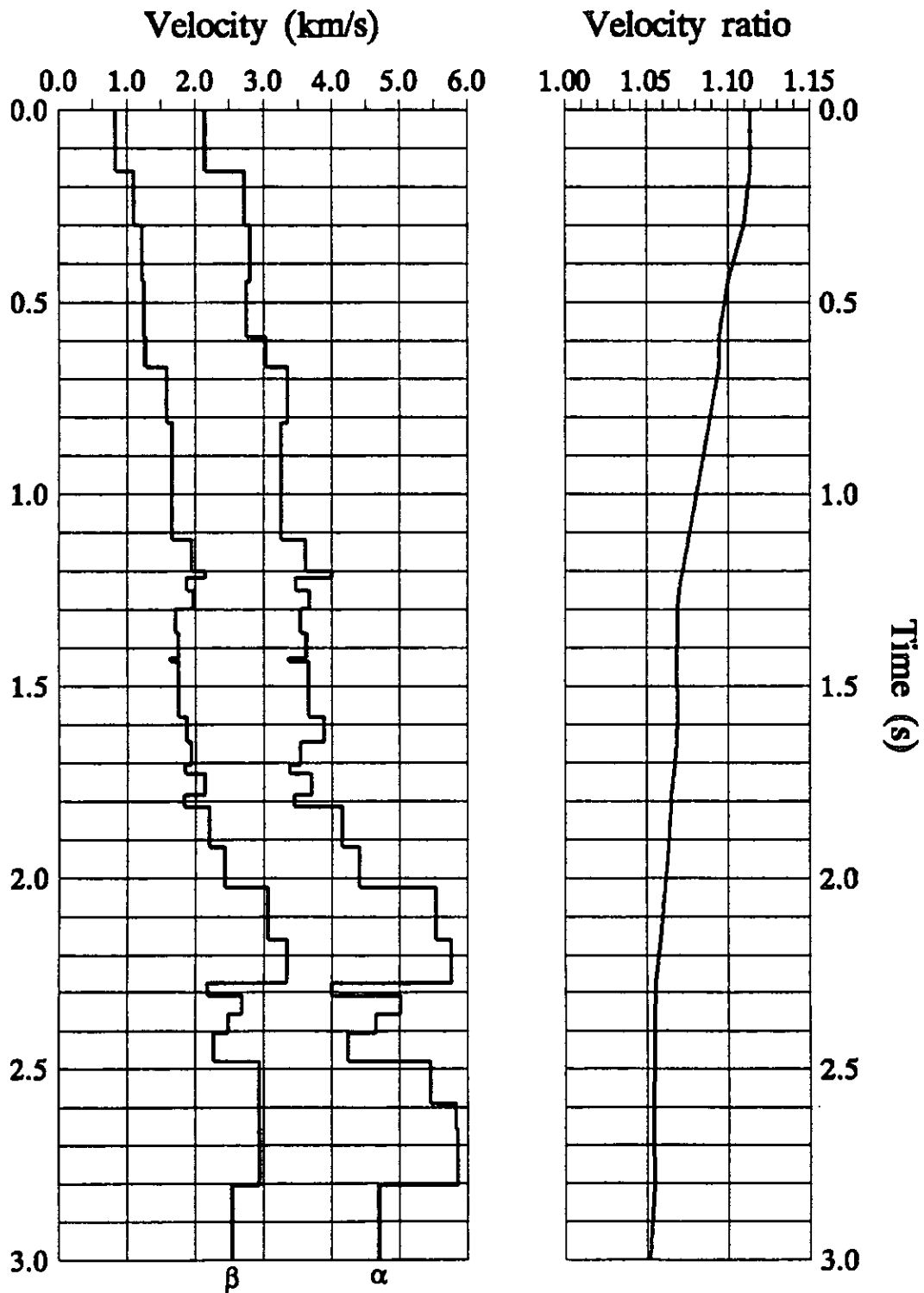


FIG. 9. Velocity model used to generate the second synthetic data set, plotted as a function of total two-way P-SV traveltime. Also shown is the ratio of RMS and migration velocity functions for this model.

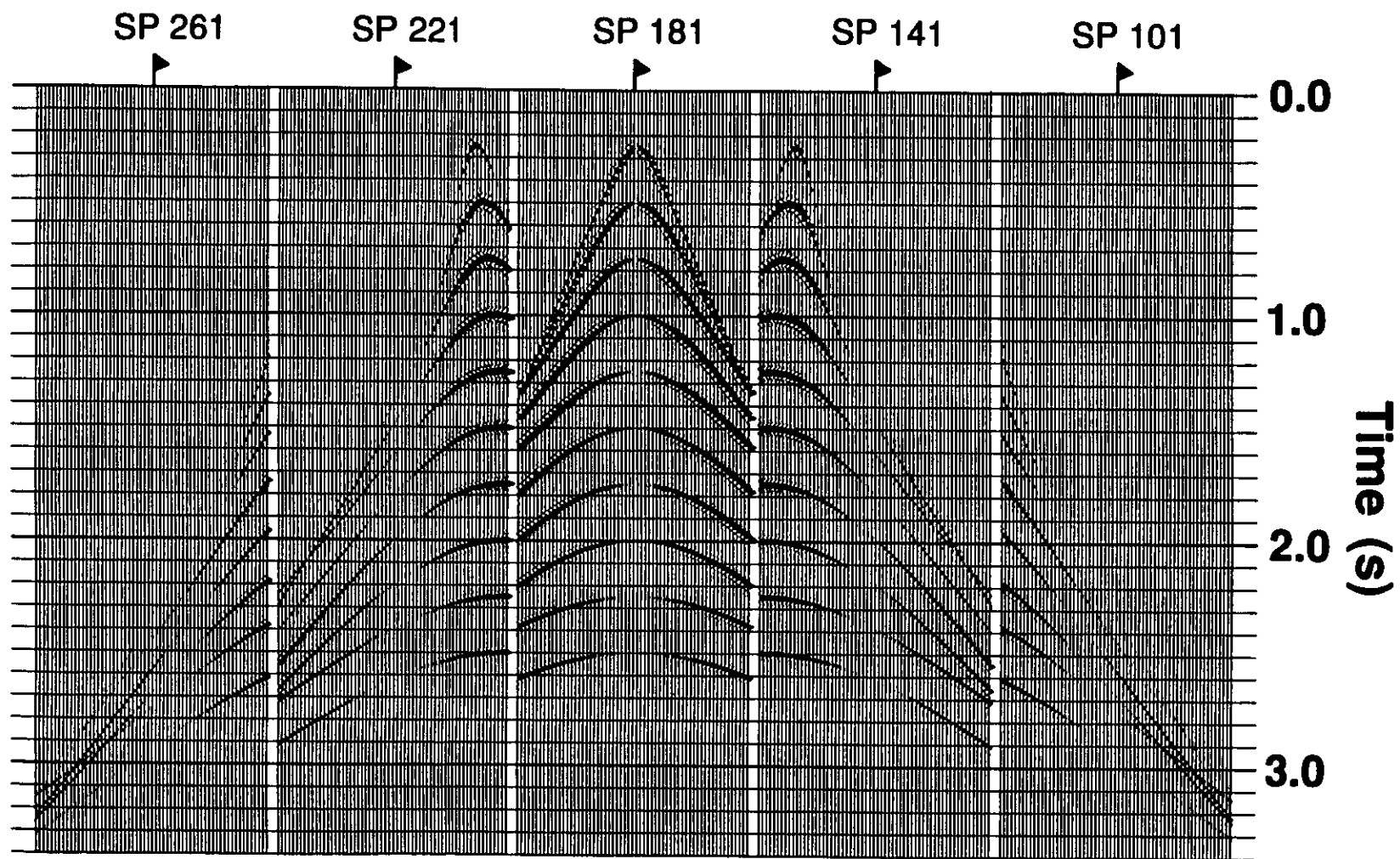


FIG. 10. Sample synthetic P-SV records for the variable-velocity case (every second trace). The data have been NMO corrected and scaled for spherical divergence.

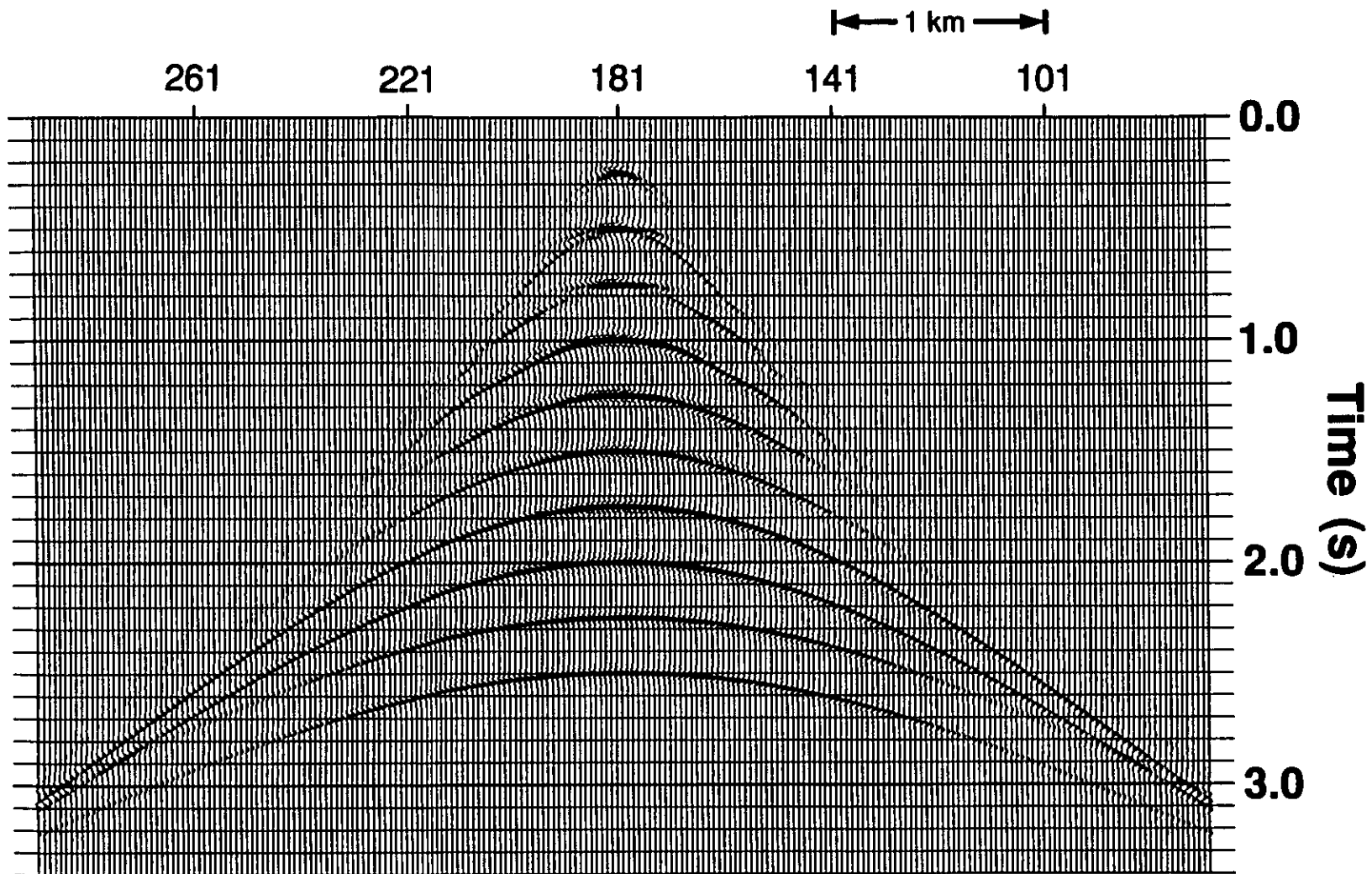


FIG. 11. Variable-velocity data stacked using DVBM (every second trace).

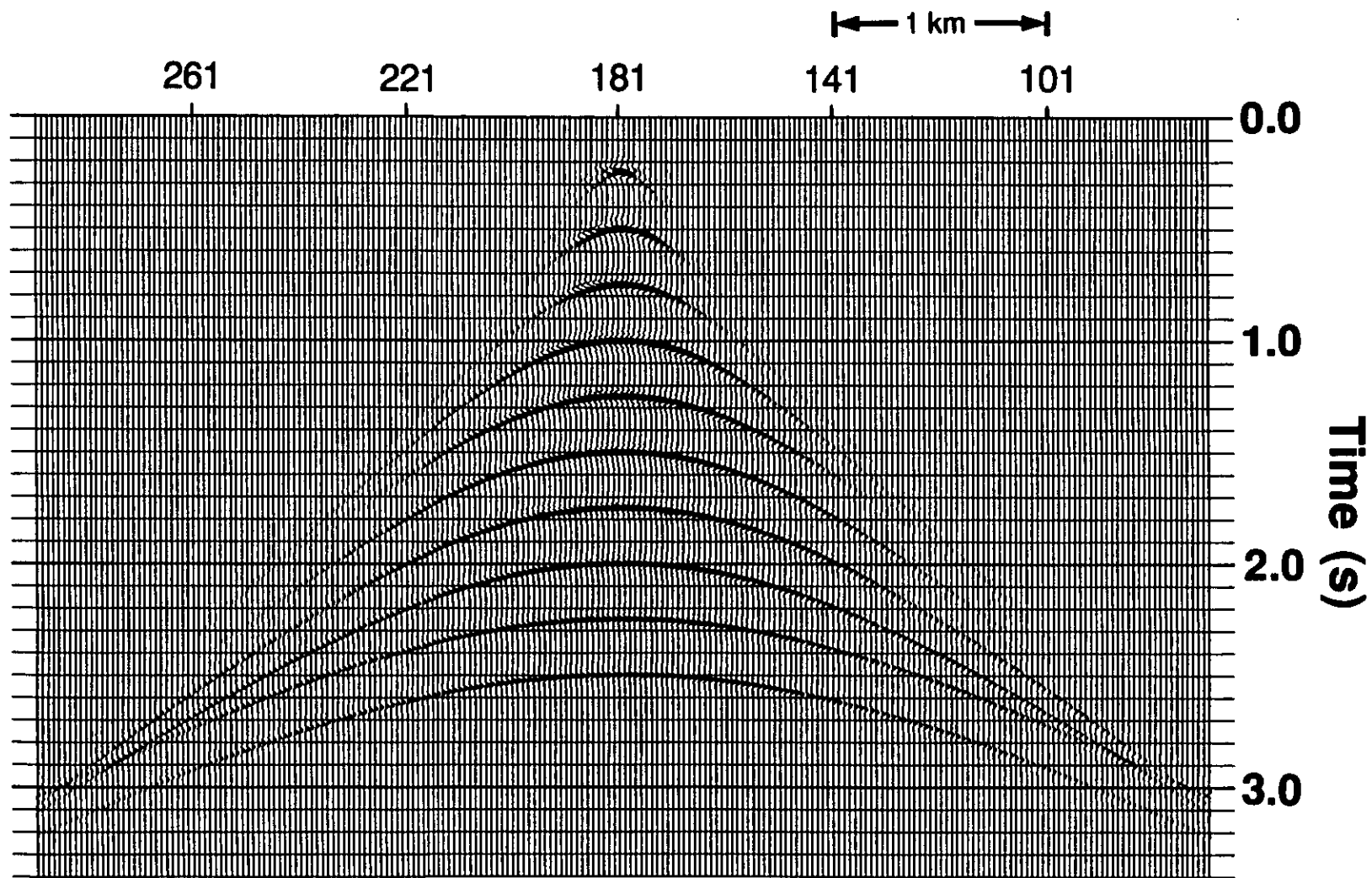


FIG. 12. Variable-velocity data stacked using depth-variant P-SV DMO (every second trace).

sourcepoints to the right of the diffractors and those to the left (Harrison, 1990), which leads to differences in apparent stacking velocity. The DMO section is again found to better preserve the diffraction tails, and the diffraction splitting is eliminated.

Phase shift migration was applied to the DVBM and DMO stack sections using the RMS velocity function, giving the results shown in Figures 13 and 14. In both cases the diffractions have been overmigrated. In addition, the first five diffractions on the DVBM section have been smeared horizontally by migration, and artifacts have been created.

The DVBM and DMO stack sections were also migrated using the migration velocity function (equation 21). The migrated DVBM section (Figure 15) again shows both lateral smearing of the shallow diffractors and the creation of migration artifacts. Migration of the DMO section (Figure 16) has successfully imaged all but the last two diffractors, which are slightly undermigrated. In further testing it was found that these two diffractors required a 2% increase in migration velocity to be completely collapsed.

DISCUSSION

The large amount of diffraction splitting that is seen in Figure 11 strongly suggests that DMO should be applied to P-SV data with any significant amount of dip. This splitting is a problem which does not occur in reflection data, and could imply that DMO can be beneficial to P-SV data in areas where it gives no noticeable improvement to conventional data.

The undermigration of the last two diffractors in Figure 16 can be understood by referring to Figure 4. There are seen to be large changes in interval velocity after 2 seconds, where these diffractors are positioned. Because the migration equation is a low-order approximation to the zero-offset travelpaths, it is probable that the large variations in ray parameter that would accompany large velocity changes make the higher order terms in equation 19 significant. The degree of undermigration is, however, seen to be small.

Although the migration velocities differ from the RMS velocities, it appears from Figure 9 that reducing the RMS velocities to about 94% of their value gives a reasonable estimate of the migration velocities for the deeper data. This could explain why poststack migration has been successfully applied to P-SV sections in the past. It should be noted that the RMS-to-migration adjustment factor is in addition to the usual 90% reduction that would be applied to stacking velocities to obtain migration RMS velocities. This gives an expected total reduction of approximately 20% for the shallow data and 16% for the deeper data.

CONCLUSIONS

It is shown here that P-SV diffractions in a vertically-inhomogeneous medium are hyperbolic to first order, and an expression for their migration velocity can be obtained. The resulting velocities are 6-11% less than the P-SV RMS velocities. Asymmetric dispersal was found to create in synthetic data a strong splitting of diffraction tails at shallow depths. Depth-variant P-SV DMO is able to remove this splitting and better preserve the diffraction tails. Migration of the DMO-corrected synthetic P-SV stack data using a conventional phase-shift algorithm and the appropriate migration velocities

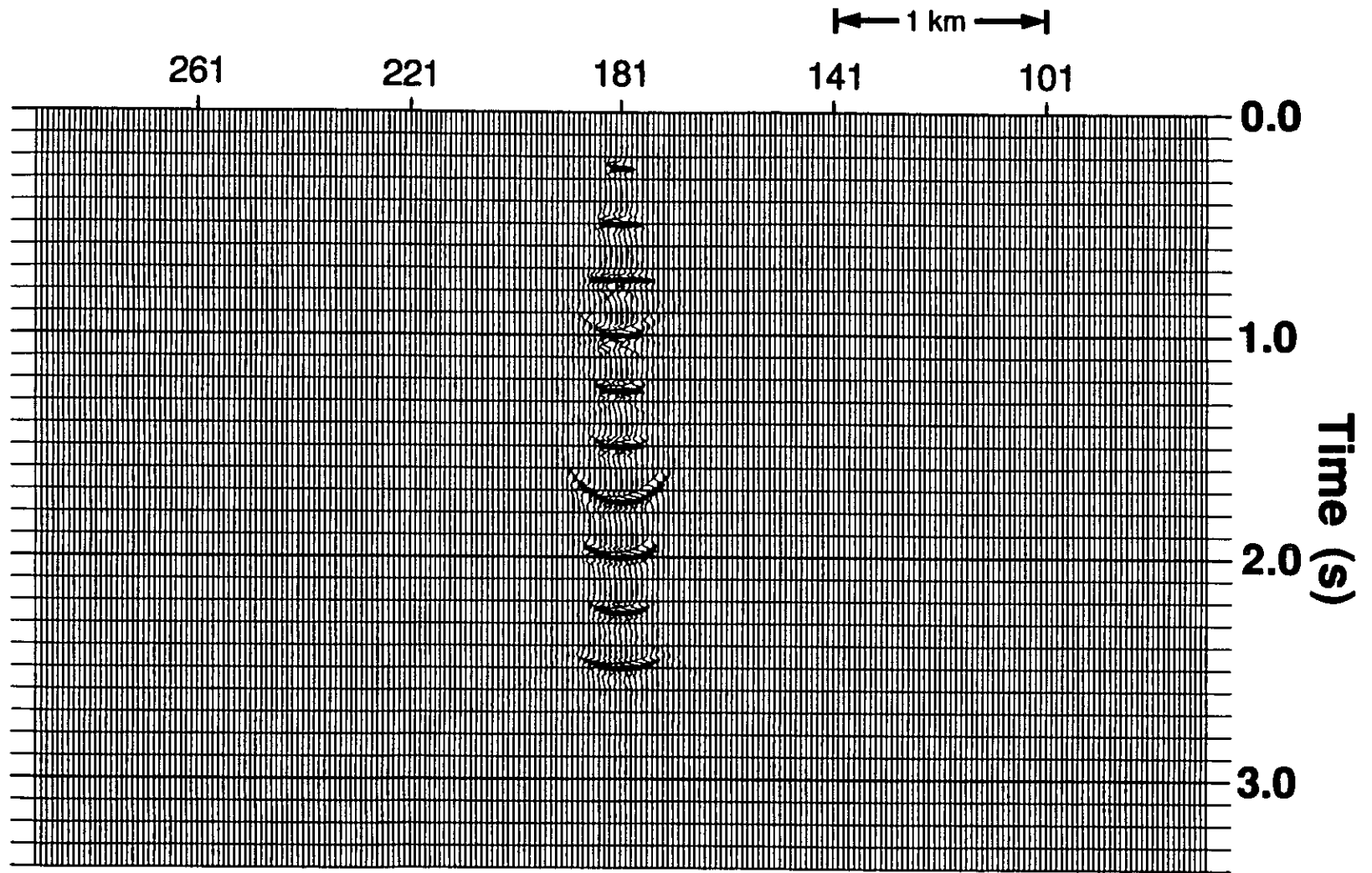


FIG. 13. DVBM-stacked variable-velocity data migrated using the RMS velocity function (every second trace).

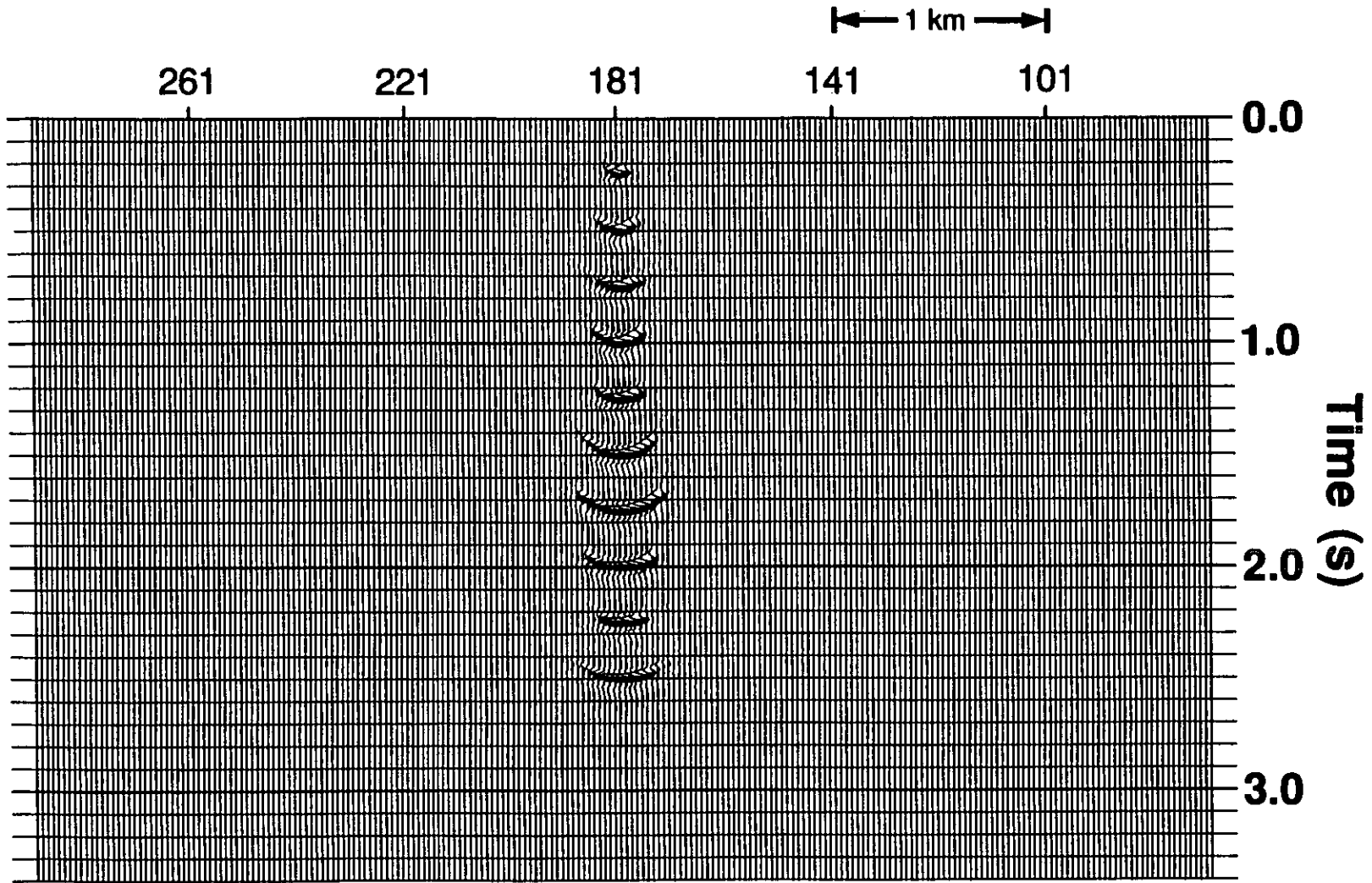


FIG. 14. DMO-stacked variable-velocity data migrated using the RMS velocity function (every second trace).

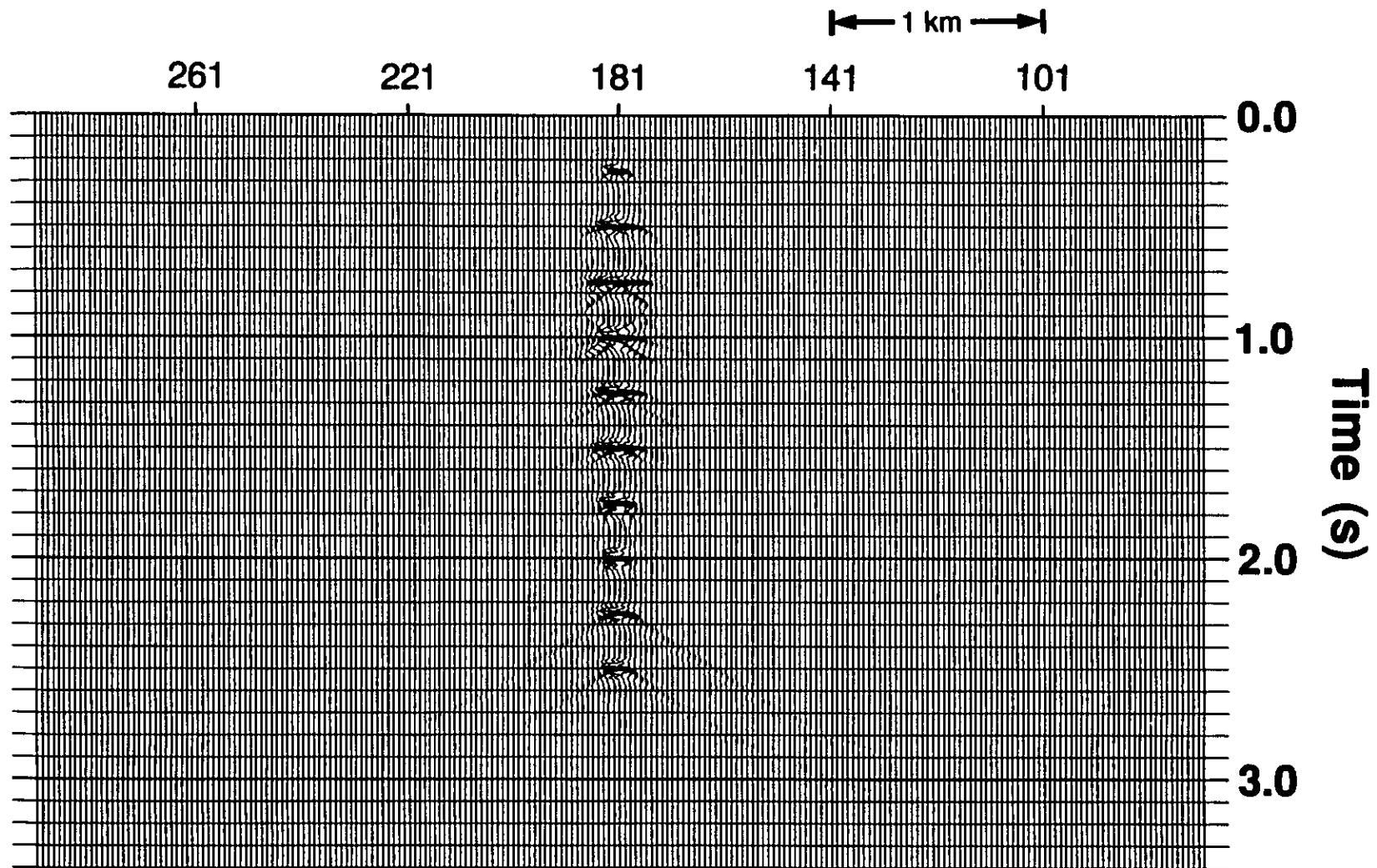


FIG. 15. DVBM-stacked variable-velocity data migrated using the migration velocity function (every second trace).

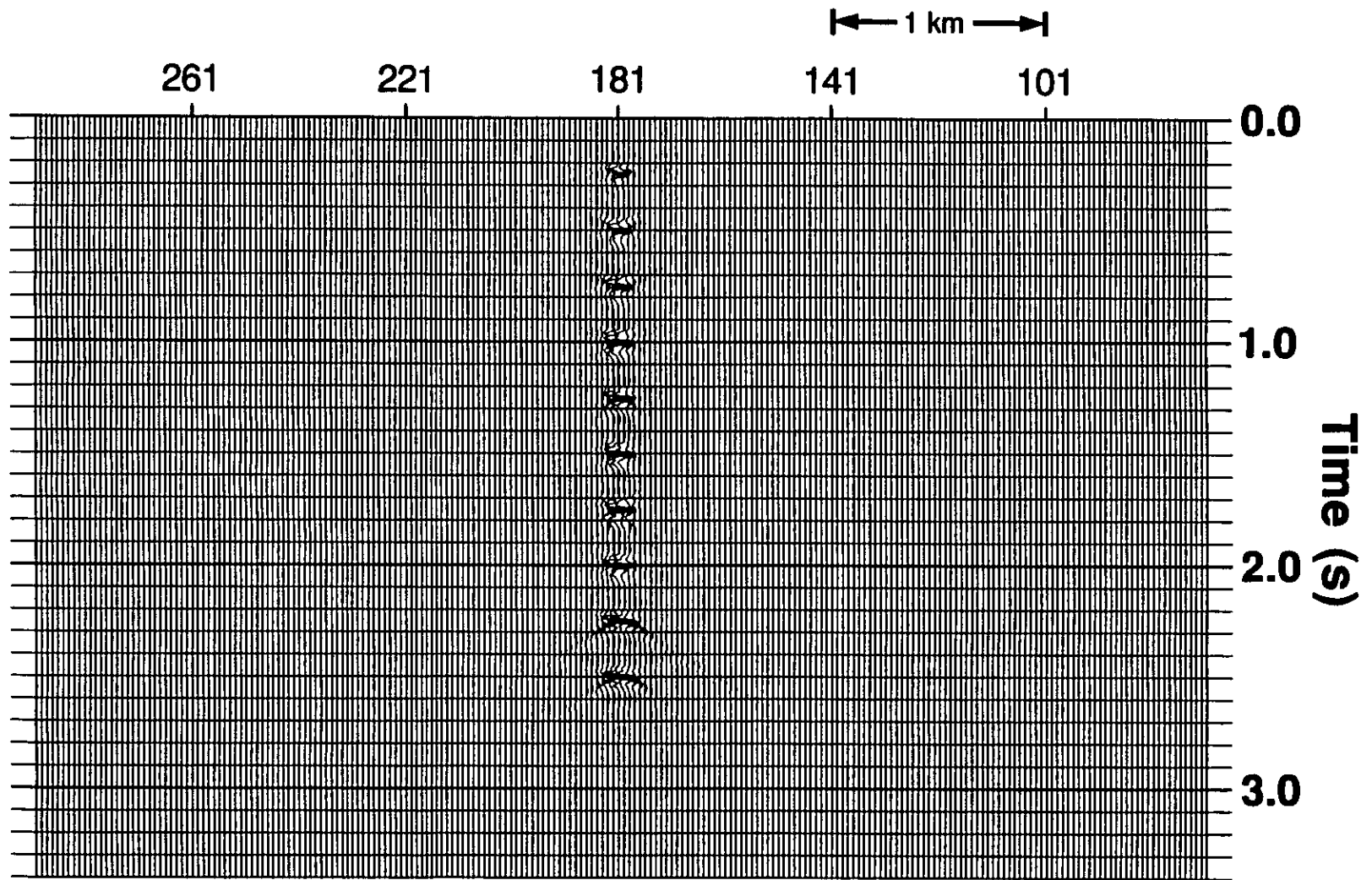


FIG. 16. DMO-stacked variable-velocity data migrated using the migration velocity function (every second trace).

adequately collapses diffractions, while migration using the RMS velocity function gives significant overmigration.

REFERENCES

- Brouwer, J., Douma, J., and Helbig, K., 1985, A new look at migration: *First Break*, v. 3, 9-15.
- Eaton, D.W.S., and Stewart, R.R., 1989, Aspects of seismic imaging using P-SV converted waves: CREWES project annual report, v. 1, 68-92.
- Eaton, D.W.S., Slotboom, R.T., Stewart, R.R., and Lawton, D.C., 1990, Depth-variant converted-wave stacking: presented at the 60th Ann. Internat. Mtg., Soc. Explor. Geophys.
- Eaton, D.W.S., Stewart, R.R., and Harrison, M.P., 1991, The Fresnel zone for converted P-SV waves: *Geophysics*, v. 56, 360-364.
- Gadzag, J., 1978, Wave equation migration with the phase-shift method: *Geophysics*, v. 43, 1342-1351.
- Garotta, R., 1986, Two-component acquisition as a routine procedure, in Danbom, S.H., and Domenico, S.N., Eds., *Shear-wave Exploration: Geophysical development series*, v. 1, Soc. Explor. Geophys., 122-136.
- Harrison, M., 1990, Dip moveout for converted-wave (P-SV) data: CREWES project annual report, v.2, 89-111.
- Knopoff, L., 1959, Scattering of compression waves by spherical obstacles: *Geophysics*, v. 24, 30-39.
- Loewenthal, D., Lu, L., Roberson, R., and Sherwood, J.W.C., 1976, The wave equation applied to migration: *Geophys. Prosp.*, v. 24, 380-389.
- Nazar, B., 1990, Multicomponent modeling of a conglomerate bar deposit: CREWES project annual report, v. 2, 204-224.
- Slotnick, M.M., 1959, *Lessons in seismic computing*: Soc. Explor. Geophys.
- Tessmer, G. and Behle, A., 1988, Common reflection point data-stacking technique for converted waves: *Geophys. Prosp.*, v. 36, 661-688.